Biomaterials 34 (2013) 1128–1134

Contents lists available at SciVerse ScienceDirect

Biomaterials

journal homepage: www.elsevier.com/locate/biomaterials

Photothermal cancer therapy via femtosecond-laser-excited FePt nanoparticles

Cheng-Lung Chen [a], Ling-Ru Kuo [a], Shin-Yu Lee [a], Yeu-Kuang Hwu [a], Shang-Wei Chou [a,b], Chia-Chun Chen [b,c], Fu-Hsiung Chang [d], Kung-Hsuan Lin [a], Dzung-Han Tsai [a], Yang-Yuan Chen [a,e,*]

[a] Institute of Physics, Academia Sinica, Taipei 11529, Taiwan
[b] Department of Chemistry, National Taiwan Normal University, Taipei, Taiwan
[c] Institute of Atomic and Molecular Sciences, Academia Sinica, Taipei, Taiwan
[d] Institute of Biochemistry and Molecular Biology, College of Medicine, National Taiwan University, Taipei, Taiwan
[e] Graduate Institute of Applied Physics, National Chengchi University, Taipei, Taiwan

ARTICLE INFO

Article history:
Received 4 September 2012
Accepted 17 October 2012
Available online 5 November 2012

Keywords:
Photothermal therapy
FePt
Nanoparticle
Cancer therapy
Thermal lens
Laser

ABSTRACT

FePt nanoparticles (NPs) have recently been revealed to be significant multifunctional materials for the applications of biomedical imaging, drug delivery and magnetic hyperthermia due to their novel magnetic properties. In this study, a newly discovered photothermal effect activated by the near infrared (NIR) femtosecond laser for FePt NPs was demonstrated. The threshold laser energy to destroy cancer cells was found to be comparable to that of gold nanorods (Au NRs) previously reported. Through the thermal lens technique, it was concluded that the temperature of the FePt NPs can be heated up to a couple of hundreds degree C in picoseconds under laser irradiation due to the excellent photothermal transduction efficiency of FePt NPs. This finding boosts FePt NPs versatility in multifunctional targeted cancer therapy.

1. Introduction

The application of thermal heat to eliminate or restrain specific cancer cells is a widely acknowledged approach in optimizing cancer therapy [1]. This non-invasive technique to eradicate tumor cells is generally referred to as hyperthermia or thermotherapy, in which the elevated temperature can promote the denaturation of intracellular protein and/or the disruption of membrane, leading to cell death. The performance of thermotherapy is mainly influenced by the power density of the applicators, and the energy absorption and thermal conductance of the biological environment. Thermotherapy has far fewer restrictive side effects than conventional chemotherapy and radiotherapy [2]. It also has greater potential in evading any developed intracellular resistance mechanism, and is beneficial in dealing with some types of malignant tumor cells.

Thermotherapy has been under investigation for some time now, the main challenge in its development is in achieving highly localized thermal effect on tumor cells with defined lesion boundaries within a short period of time. Recently, thermotherapies based on NIR irradiation–activated nanomaterials have received significant attention due to their efficacy in destroying cancer cells. In particular, because of their unique optical and thermal properties, gold and carbon based nanomaterials gained significant interest [3–8]. Nonetheless, the approach is by no means perfect, and the investigation into exploring superior materials and methodology is still imperative. In this study, we present the possibility of using magnetic FePt NPs excited by NIR femtosecond laser for aforementioned tumor-targeted therapy. FePt NPs have recently gained recognition as a superior material in cancer diagnosis and therapy [9–11]. The excellent superparamagnetic property and high X-ray absorption of FePt NPs make it a potential dual modality contrast agent for computed tomography (CT) and magnetic resonance imaging (MRI). The transport and/or immobilization of magnetic nanoparticles to a targeted region of a tumor can be easily manipulated by an external magnetic field gradient. Similarly, the magnetic FePt NPs can respond resonantly to an external AC magnetic field and result in a controllable heating effect, serving as hyperthermia agents delivering thermal energy to targeted tumors. Thus, FePt NPs present an opportunity in realizing CT, MRI, magnetic–thermal, and photothermal treatments all within a single agent. The benefits of such versatility should make FePt NPs, or similar materials, competitive candidates in future cancer therapies.

* Corresponding author. Institute of Physics, Academia Sinica, Taipei 11529, Taiwan. Tel.: +886 2 27896725; fax: +886 2 27834187.
E-mail address: cheny2@phys.sinica.edu.tw (Y.-Y. Chen).

0142-9612/$ – see front matter © 2012 Elsevier Ltd. All rights reserved.
http://dx.doi.org/10.1016/j.biomaterials.2012.10.044

FePt NPs were chemically synthesized and functionalized with folates to target breast cancer cells EMT-6. When subjected to activation by NIR femtosecond laser, we discovered that FePt NPs triggered considerable intracellular explosions, which resulted in the perforation and/or sudden rupture of the plasma membrane. The distinctive thermal–optical property of FePt NPs was further investigated using thermal lens spectroscopy. The energy fluence threshold for cancer cells destruction and the photon-to-heat conversion efficiency of FePt NPs were compared with that of Au NRs.

2. Materials and methods

2.1. Preparations of FePt NPs

The FePt NPs were prepared through confined decomposition of $Fe(CO)_5$ (iron pentacarbonyl, Fluka, 99%) and reduction of $Pt(acac)_2$ (platinum acetylacetonate, ACROS, 97%) in the presence of oleic acid (Aldrich, 90%) and oleyl amine (Aldrich, 70%) [9,12]. Briefly describing, $Pt(acac)_2$, 1,2-hexadecandiol (Aldrich, 90%), dioctyl ether (ACROS, 90%), $Fe(CO)_5$, oleyl amine and oleic acid were mixed and heated to 240° C. After several minutes, the reaction mixture was cooled to room temperature. The black product was separated by adding ethanol and centrifugation. The final product was stored in hexane or toluene, and the water-soluble NPs were obtained by the following ligand-exchange procedures. The dry FePt NPs were then redispersed in a mixture of Dimethylsulfoxide (DMSO, Sigma) and 3-mercaptopropionic acid. Then the nanoparticles were separated by centrifugation, and the precipitate was dispersed in water (pH ~12). The UV–visible absorption spectra of nanoparticles were obtained by the spectrophotometer (Spectronic, GENESYS-8), and the size and morphology of nanoparticles were analyzed on a Philips/FEI Tecnai 20 G2 S-Twin transmission electron microscope.

2.2. Preparation of the folate-conjugated FePt NPs

The folate-conjugated FePt NPs were prepared by conjugating the nanoparticles with carboxyl group with folic acid. These nanoparticles were first activated with *N*-ethyl-*N* 8-(dimethylaminopropyl)-carbodiimide (EDC), and then folic acid was added and stirred for at least 12 h at room temperature. The folate-conjugated nanoparticles were then separated by centrifugation and washed several times.

2.3. Cell culture and cell viability assay (MTT)

EMT-6 cells were cultured in folic acid free medium to ensure overexpression of folate receptors on the surface of the cells. To determine the cytotoxicity of nanoparticles, the cell viability is generally quantified by colorimetric assay. Briefly, the number of living cells is directly proportional to the absorbance of formazan which was produced from the mitochondrial oxidation of 3-(4,5-dimethylthiazolyl-2)-2,5-diphenyltetrazolium bromide (MTT) in living cell. EMT-6 cells were harvested after passage and plated at a density of 1.25×10^5 cells/mL in 96-well plates with 300 μL medium (100 μL/well), and incubated at 37° C under a 5% CO_2 atmosphere for 24 h. After that, these cells were further incubated for 24 and 48 h with 3-mercaptopropionic acid-modified FePt at varying concentrations; these were then treated with a freshly prepared 12 mM MTT solution (10 μL) and incubated for an additional 3 h. Next, MTT solution was removed and 50 μL of DMSO was added to each well. The wells were left for 30 min in the dark, and then assayed with an automated reader, the absorbance was fixed at 570 nm. The acquired cell viability was expressed as a percentage relative to cells incubated with medium only.

2.4. Femtosecond laser triggered photothermolysis of cancer cells

The photothermolysis of cancer cells was performed on an inverted scanning microscope (LSM510, META/Observer, Z1, Zeiss). A femtosecond (fs) Ti:Sapphire laser (Spectra-physics MaiTai HP) with a duration time of 100 fs, linearly polarized and with a repetition rate of 80 MHz was equipped in the microscope as the excitation source. The wavelength and average power of the laser beam were tunable, and a water-immersion objective lens (NA = 1.4) was used. For photothermolysis studies, the centered wavelength can be tuned from 700 to 990 nm, an area of $90 \times 90\ \mu m^2$ (512×512 pixels; each pixel area = $176 \times 176\ nm^2$) was scanned at a relatively slow exposure time of 164 μs per pixel per scan to activate FePt NPs. The exposure time of nanoparticles was calculated following the established method [13]. In this work, one scan of two different excited power densities (148 and 19 W/cm^2) were applied to the objectives. The calculated energy fluences were about 70 and 10 mJ/cm^2, respectively.

2.5. Preparation of cell specimens for electron microscopy

The EMT-6 cells were cultured in a Petri dish and treated by trypsins. Next, the cells were fixative and pelleted by a series of standard protocol. Then, cell pellets were post-fixed in OsO_4 solution, washed and finally dehydrated in ethanol series and acetone. The samples were further hardened under the procedure of infiltrating in Spurr's embedding mediums. The ultrathin sections were cut by using an ultramicrotome (LEICA, EM, UC6), and stained with uranyl acetate and lead citrate for observation by a transmission electron microscope (Hitachi, H-600).

2.6. Thermal lens spectroscopy

100 fs pump pulses (800 nm, 80 MHz) were focused to the samples with a 30 cm lens. The incidence power was ~30 mW, and the diameter of the focused spot was ~0.22 mm. The pump beam was modulated with a chopper, which controls the exposure time. The chopping frequency varies between 10 Hz and 400 Hz in the experiment. Another 638 nm continuous-wave lasers (probe) were focused with a 20 cm lens, and the incidence power was attenuated to 0.2 mW. The focal point was 2 cm in front of the samples, and the diameter of the spot was ~0.13 mm. The diverging probe beam (after the focal point) was carefully aligned to overlap with the pump spot at the sample. A photodiode (with active area 0.8 mm^2) was placed ~2 m behind the sample to measure the intensity at the center of the diverged spot. The electrical signal from the photodiode was demodulated with a lock-in amplifier.

3. Results and discussion

3.1. Characterization of FePt nanoparticles

Cubic-like shaped FePt NPs with a face-centered cubic structure were prepared by the thermolysis of metal-organic precursors and surfactant-assisted methods [9]. The average size of the prepared FePt NPs is 12 ± 1.0 nm in diameter, and its alloying composition is found to be $Fe_{34}Pt_{66}$ (Fig. 1). To characterize the magnetic properties of FePt NPs, a superconducting quantum interference device (SQUID) was employed to measure their magnetic properties. In the inset of Fig. 2a, the superparamagnetic behaviors of FePt NPs with blocking temperature (T_B) ~ 100 K is shown, and the magnetic field dependence of magnetization below and above T_B is revealed (Fig. 2a). To have FePt NPs suitable for biological applications, a ligand-exchange procedure was performed on FePt NPs to displace the original surfactants on the nanoparticles' surface. Here, 3-mercaptopropionic acid (MPA) was chosen to produce COOH-terminated water-dispersible FePt NPs [14]. The surfaces of MPA-FePt NPs were then modified with folic acid to specifically target folate receptors that are often overexpressed in breast, lung, colon

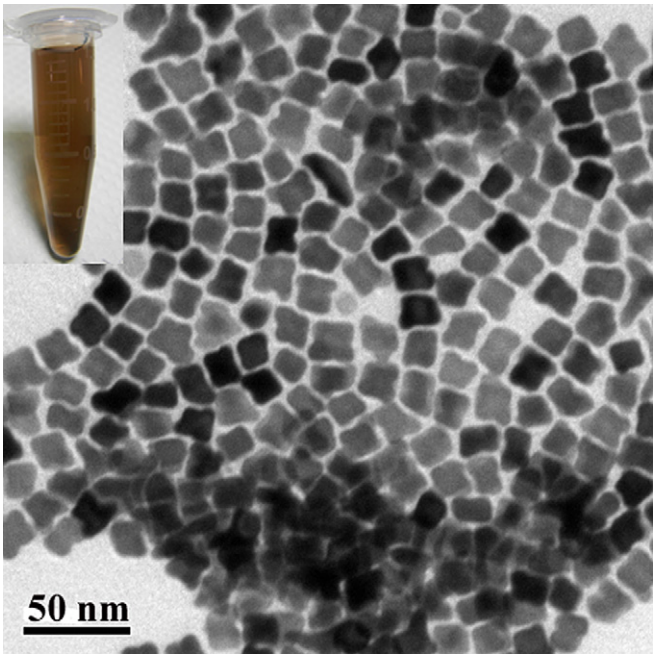

Fig. 1. The TEM image and solution color feature of FePt NPs.

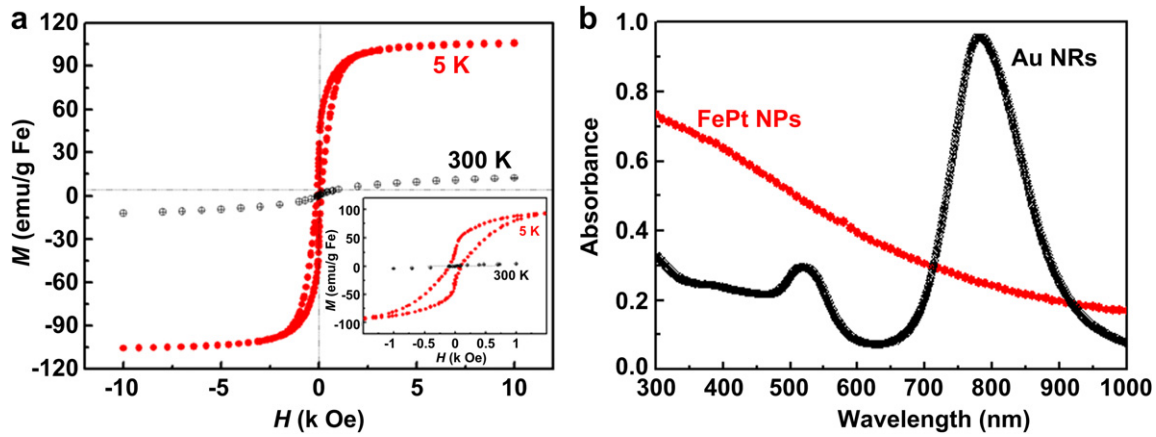

Fig. 2. (a) The magnetization versus field for FePt NPs at 5 and 300 K respectively. The inset is an enlargement of low field region. (b) Absorption spectra of folate-conjugated FePt NPs and polystyrenesulfonate capped Au NRs with aspect ratio 3.9 and 40 nm in long axis. Peaks at 525 and 780 nm represent plasma resonance of Au NRs [18].

cancer cells [15]. Fig. 2b shows the absorption spectra of FePt NPs and Au NRs. For FePt NPs, instead of the unique feature of plasmon resonance as that of Au NRs, a broadband absorption at NIR region was observed. To directly examine the photothermal effect of FePt NPs, an experiment with a very simple design was conducted. Firstly, FePt NPs were dispersed in water and sealed in a home-made microchamber which is a 5 × 5 mm^2 groove with 10 μm in depth. As FePt NP agglomerates were irradiated by 100 fs laser with $\lambda = 800$ nm, an energy threshold of ~85 mJ/cm^2 was obtained for the immediate generation of microbubbles (Fig. 3). It is known that the formation of explosive vapor bubbles on FePt NPs surely requires an elevated temperature higher than the critical temperature of the water [16]. Therefore, we speculate that the temperature of FePt NPs should be transiently heated to a couple of hundred degrees Celsius and/or reach their melting point during NIR femtosecond laser pulse irradiation. The localized accumulated heat would also cause the thermal disassembly of FePt NP agglomerates into smaller fragments, and dispersed to the surroundings. Although such explosive evaporation process occurred within a nanosecond [17], the nature of the phenomenon can be confirmed from formed bubbles trapped in the chamber. Contrastingly, in a control experiment with no nanoparticles, no microbubble could be detected, even with laser intensity up to 1000 mJ/cm^2. The proposed mechanism is further supported by transmission electron microscopy (TEM), wherein featureless fused FePt agglomerates were observed; an expected result of local heating.

3.2. Cellular uptake and biocompatibility of FePt nanoparticles

FePt NPs were then introduced into cellular environment. The TEM micrograph shows that the cellular framework was well preserved with no visible abnormalities following incubation of FePt NPs for 4 h (Fig. 4a). Most of the ingested folate-conjugated FePt NPs were found to gather into numerous clusters in several large vesicular structures. The ingested numbers of FePt NPs in each cluster are around several thousands to ten-thousands. On average, several ten-thousands of nanoparticles were taken up per cell. An analogous phenomenon was also observed in similar experiment with Au NRs [18], and such accumulation of nanoparticles into clusters has been proven profitable in the reduction of laser energy threshold due to collective heating effects [19,20]. Furthermore, cell viability assays revealed no adverse toxicity effects on live EMT-6 breast cancer cells after their exposure to various concentrations of FePt NPs (5–100 μg/mL) for 24 and 48 h (Fig. 4b). These results thus justify their biocompatibility to further *in vitro* and *in vivo* photothermal therapeutic investigations.

3.3. In situ real-time observation of selective photothermolysis in cancer cells

To investigate the details of photothermal effect of FePt NPs *in vitro*, a linearly polarized pulsed laser was employed to irradiate nanoparticles at a repetition rate of 80 MHz, and the simultaneous transition of cellular nucleus was monitored by the fluorescent dye

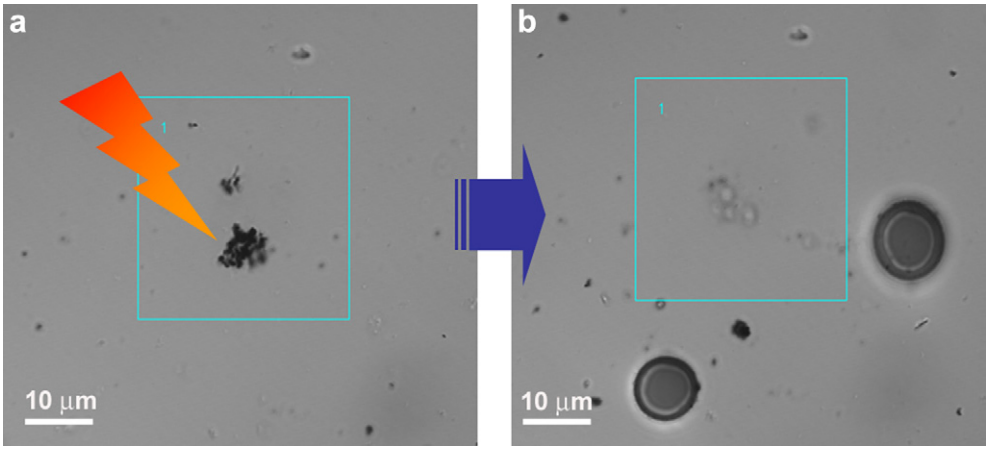

Fig. 3. Bright-field micrographs of FePt NP solution before (a) and after (b) pulsed laser excitation, respectively. The black circles are water bubbles.

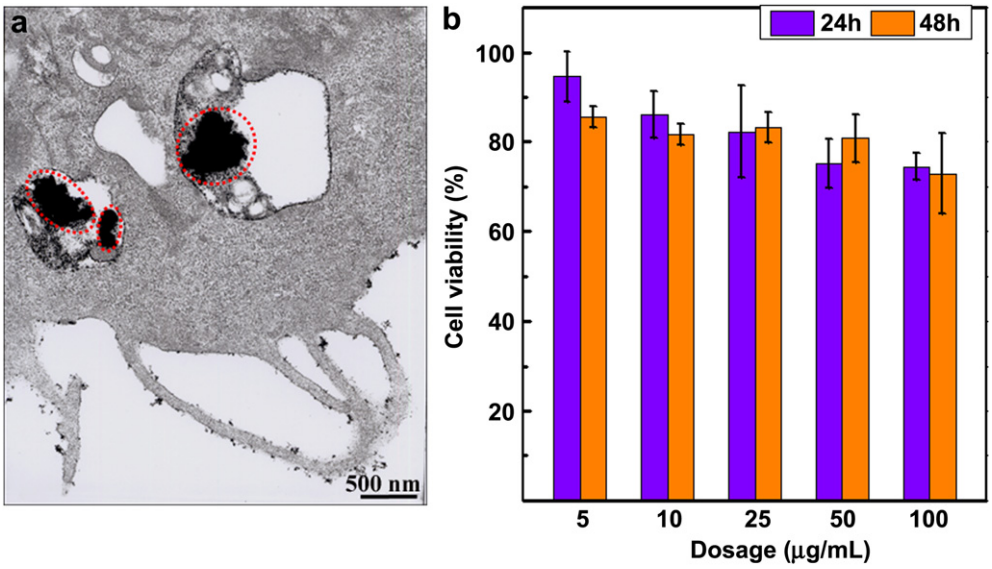

Fig. 4. (a) The TEM micrograph of partial fixed cell showing few clusters of FePt NPs (marked by red circles). On average, the size of FePt NP cluster is about 1–3 μm. (b) Cell viability of EMT-6 cells exposed to FePt NPs after 24 and 48 h incubation. The viability of the cells was normalized with respect to a media-only control. (For interpretation of the references to color in this figure legend, the reader is referred to the web version of this article.)

exclusion method [18]. Typically, two dyes, YOPRO-1 (green coloring) and propidium iodide (red coloring) are used to qualitatively indicate plasma membrane integrity of the cells. EMT-6 cancer cells without FePt NPs were initially irradiated in order to determine the secure energy fluence of laser irradiation. It was found that EMT-6 cells survived with laser powers not exceeding 110 mJ/cm^2: a value that is slightly above the established safety standard of 100 mJ/cm^2 for medical lasers [21]. For cells incubated with FePt NPs, subjected to such high powers, cells with trace of FePt NPs were completely destroyed through a process resembling an instantaneous internal hyperthermic explosion. A series of confocal images, taken with a 60 s frame rate, of cells incubated with FePt NPs ($N \sim 6$–10 clusters) and exposed to a reduced laser energy fluence of ~70 mJ/cm^2 (power density = 148 W/cm^2 and time duration = 505 μs), showed a discernible explosion phenomenon along with the formation of characteristic cavities in the targeted cell, especially near nanoparticle agglomerates (Fig. 5). The loss of cellular membrane integrity was finally verified from dual-color staining of the nucleus. Further reduction of laser power revealed that an energy threshold of ~10 mJ/cm^2 was sufficient for the generation of microbubbles, and killed cells ingested with relatively higher numbers ($N \sim 30$–60) of FePt NP clusters (Fig. 6). In this case, the intracellular detonations and injuries of plasma membrane were milder than those caused by higher energy fluences, yet it was still effective in damaging cancer cells. The destruction process and physiological symptom of the cell are very similar to that observed in the hyperthermia inflicted with Au NRs, i.e., the process initiates with an oncosis, along with cellular swelling, blebbing and increased membrane permeability, and finally leading to necrosis. It is noted that the results from laser exposures with other different laser wavelengths (700, 900, and 990 nm) at constant power level showed that the intracellular explosion was independent of excitation wavelengths. Specifically, the characteristic processes were observed in all cases.

3.4. Thermal lens spectroscopy of FePt nanoparticles

In order to understand how the laser's energy was adsorbed by FePt NPs, and the mechanism in which this absorbed energy dissipates into the surrounding solution inevitablly killing cancer cells in its vicinity, a specially designed thermal lens spectroscopy experiment was conducted on a FePt NPs solution to measure their optical absorption and photothermal transduction efficiency [22,23]. The FePt NPs that dispersed in deionized water were irradiated with the femtosecond laser (λ = 800 nm and ~1 μJ/cm^2 per pulse). As the photons were captured by FePt NPs, some photon energy was transferred to heat, the heat from the high-temperature nanoparticles then dissipates to the surrounding medium. A temperature rise in the sample solution will change the refractive index of solution, which becomes an acting "thermal lens". Meanwhile, another weak continuous-wave (C.W.) laser with λ = 638 nm was directed through the heated region as a temperature probe according to its central intensity which was modulated due to the optical diffraction from the thermal lens (Fig. 7a). Fig. 7b shows the intensity variation of probe beam versus laser exposure time of the FePt NP solution. The temperature rises with longer exposure time, and thus the intensity change of the optical probe increases. The sublinear relation of the curve in Fig. 7b results from heat diffusion during the exposure time. According to the theoretical model developed by Snook et al. [23], the thermal lens signal can be expressed as the following equation:

$$\frac{\Delta I(t)}{I} = 1 - \left[1 - \frac{\theta}{2}\tan^{-1}\left(\frac{2mV}{\left[(1+2m)^2+V^2\right](t_c/2t)+1+2m+V^2}\right)\right]^2 \quad (1)$$

in which

$$\theta = \frac{P_a(dn/dT)}{\kappa\lambda_p} \quad (2a)$$

and

$$t_c = \omega_e^2\rho C/4\kappa \quad (2b)$$

In Eqs. (1) and (2) I is the intensity without pump excitation, $\Delta I(t)$ is intensity drop with pump exposure time t, m is the area ratio of probe to pump at the sample, V is the ratio of distance of probe focal point (from the sample) to the confocal distance of the probe, dn/dT is the differential of refractive index of solution to temperature, P_a is the optical power which is converted to heat, λ_p is the wavelength of probe, and ω_e is the radius of the focused pump spot.

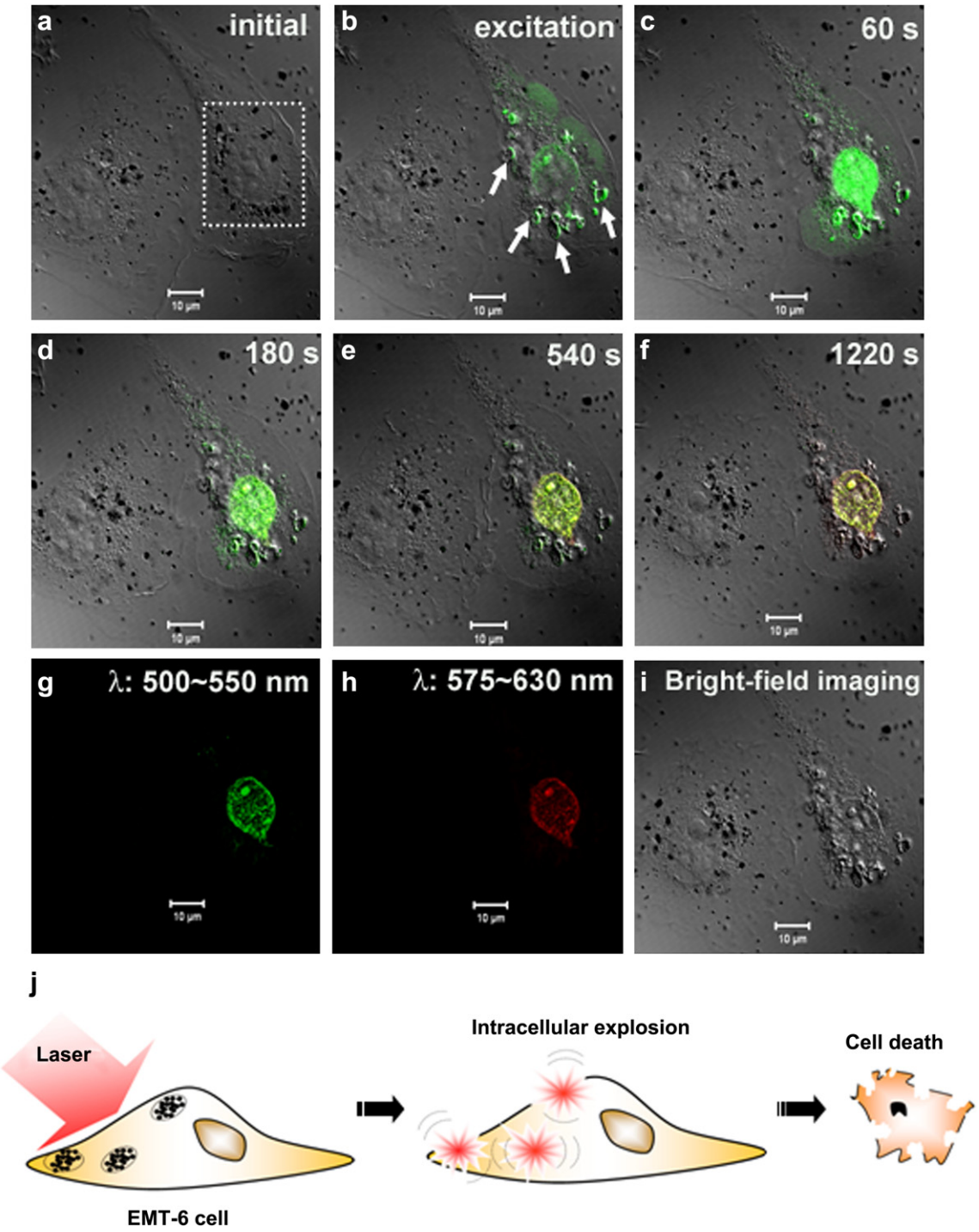

Fig. 5. Photothermolysis of the EMT-6 cancer cell triggered by FePt NPs under energy fluence of ~70 mJ/cm^2 (a–f) the laser activation area is marked with dash line, and the black dots within this region are the FePt NP clusters. After laser excitation, the cellular membrane exhibited perforation and blebbing. (g–i) At 1220 s, the confocal images were analyzed from the fluorescent signals and bright-field imaging. The red and green colorings correspond to propidium iodide and YOPRO-1 dyes, respectively. (j) Schematic representation of the photothermolysis of cancer cells mediated by laser-activated FePt NPs.

κ, ρ, C are thermal conductivity, density, and specific heat of the solution, respectively.

By fitting the experimental data (Fig. 7b), P_a for FePt NPs was determined. On the other hand, the extinction power (P_e) was measured by directly recording the powers before and after the samples, which is typically used to define the absorbance of the sample. Here, photothermal transduction efficiency η is defined by P_a/P_e. The photothermal transduction loss could result from luminescent loss and scattering loss. The parameters obtained from the thermal lens experiment are listed in Table 1, and the η of FePt NPs is about 30%. Same result was also obtained for FePt NPs solution with twice concentration. For Au NRs the measured η (20%) is very consistent with the literature value [24]. The lower η for Au NRs may be attributed to strong plasmonic scattering loss. While the electrons in Au NRs oscillate with the incident electric field of light, they also act like an antenna to re-irradiate electro-magnetic waves out to all directions, i.e. plasmonic scattering. Since the optical wavelength is at the plasmon resonance of Au NRs, plasmonic

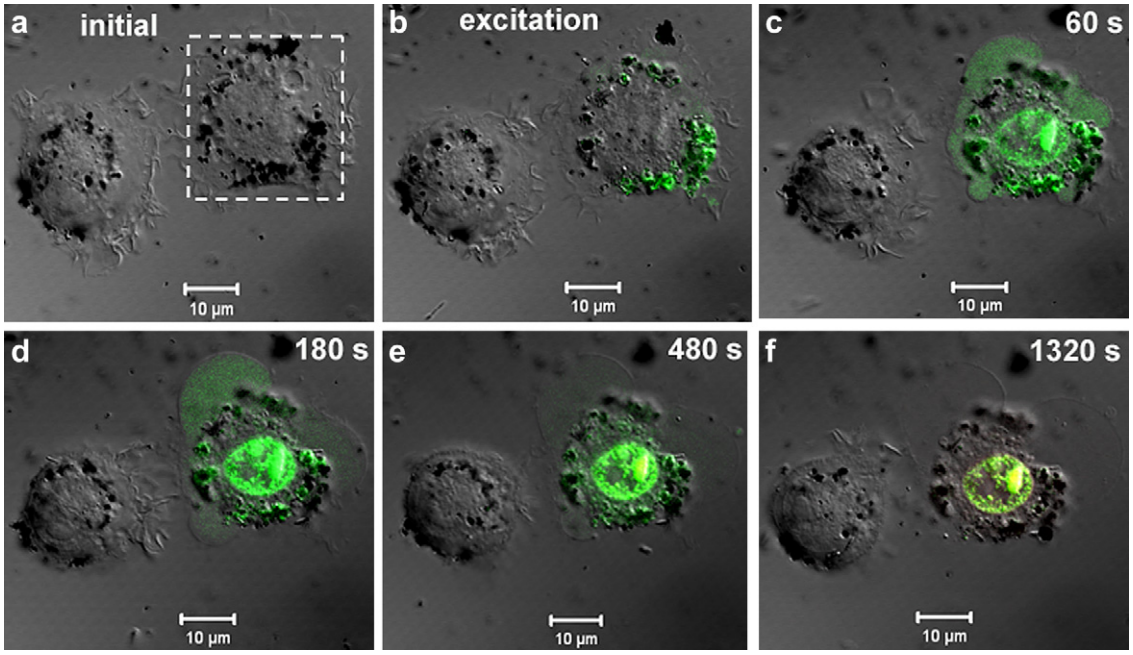

Fig. 6. Photothermolysis of the EMT-6 cancer cell triggered by FePt NPs under energy fluence of ~10 mJ/cm^2.

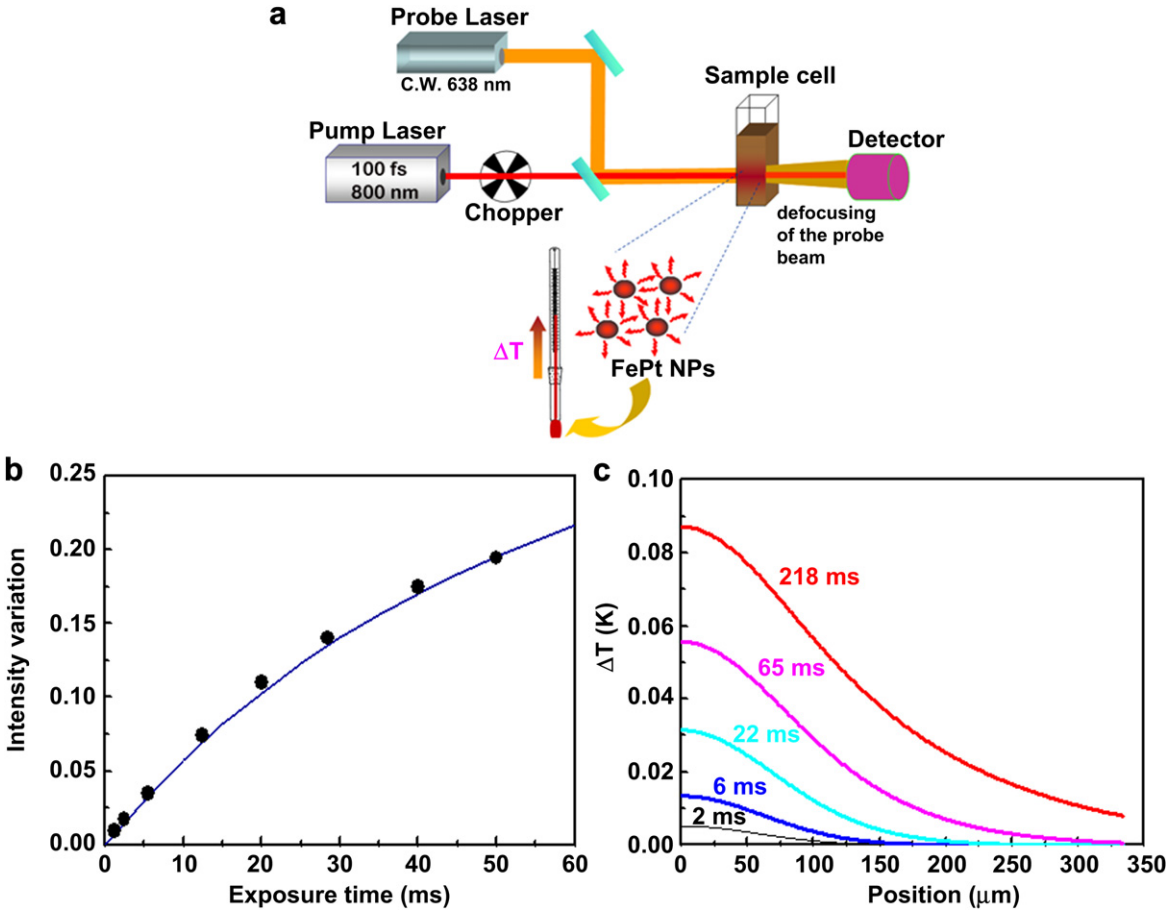

Fig. 7. Thermal lens spectroscopy for heat measurement in FePt NPs solution. (a) Schematic representation of the thermal lens technique. (b) The intensity variation of probe beam versus exposure time of femtosecond laser for FePt NPs solution. The solid line represents curve fitting. (c) The derived profile of temperature rise versus distance from center for various exposure times.

Table 1
The absorbed power to heat (P_a), the extinction power (P_e), and the calculated photothermal transduction efficiency (η) for FePt NPs and Au NRs.

	FePtNPs (80 μg/mL)	FePtNPs (40 μg/mL)	AuNRs (40 μg/mL)
P_a(mW)	4.2	2.2	5.7
P_e(mW)	13.9	7.2	28.4
η(%)	30	30	20

scattering is enhanced, which essentially contributes to the extinctive power, but does not contribute to heating.

It should be noted that the thermal lens spectroscopy was operated at relatively low fluence ($\sim$1 μJ/cm^2 per pulse) for stable measurement of light to heat conversion. According to the experimentally obtained parameters, the profiles of temperature rise of FePt NP solution were calculated for various exposed time (Fig. 7c). The temperature rises were on the order of 0.1 K with our experimental condition. For practical photothermal therapy, the fluence of the femtosecond pulses is ranged from 10 to 100 mJ/cm^2 per pulse which is 4–5 orders higher than the measurement condition and can generate much higher temperature to create microbubbles in tissues [20]. It was theoretically estimated that single femtosecond pulse (with optical density above 1 mJ/cm^2) can heat a Au NR to over 1000° C within 1 ps, and the temperature of the surrounding water at the particle surface (in nanoscale regime) can reach over 100° C after several tens of picosecond [25].

We further compared the efficacy of FePt nanoparticle photothermal therapy in cancer cells with typical plasmonic Au NRs. Comparisons were made on the basis of microbubble-formation thresholds, which play a crucial role in selective photothermolysis of cancer cells targeted with nanoparticles [20]. Under nearly the same uptake amount of $\sim 10^{-12}$ g nanoparticles per cell (based on the TEM and confocal laser scanning microscopic images), the FePt NPs' bubble-formation threshold ($\sim$10 mJ/cm^2) is almost 80% lower than that of Au NRs ($\sim$18 mJ/cm^2) [18]. This fact makes FePt NPs very promising in the laser treatment of cancer. The higher bubble-formation threshold of Au NRs, was conjectured to be that as Au NRs were heated above the melting temperature, they change their shape from rod to sphere which not only has less the absorption cross section ($\sim$36%) but also significantly shift the longitudinal surface plasmon resonance absorption peak away from NIR region [26]. Moreover, the relative lower photothermal transduction efficiency of Au NRs is also another concern. In contrast, FePt NPs could consistently convert light to heat regardless of the changes of shapes and refractive index of the surrounding media.

4. Conclusions

The *in situ* real-time observations show that localized photothermal effects of FePt nanoparticles are sufficiently high in triggering considerable intracellular explosion, and result in the perforation and/or sudden rupture of the plasma membrane. The energy fluence required to destroy cancer cells greatly depends on the number of nanoparticles within the cell. And in general, in cells with nanoparticles, the applied energy fluence is much lower than the medical safety level. Furthermore, the thermal lens spectrometry was applied to study the photothermal heating phenomena of FePt NPs, and several factors that influence the photothermal transduction efficiency of nanoparticles were discussed. This work presents an encouraging potential of utilizing FePt NPs assisted with ultrafast laser for the purpose of photothermal cancer therapy.

Acknowledgments

This work was supported by the National Science Council of the Republic of China under Grant No. NSC 100-2120-M-001-0019-MY3. We thank Mr. Hong-Chi Chen for his help with microchamber fabrications, Dr.Chi-Keung Chan for his help with UV–visible absorption spectra analysis, Ms. Shu-Chen Shen for her help with confocal imaging analysis, and Mr. Cheng-Kuang Huang for his important contribution to the research effort.

References

[1] Wust P, Hildebrandt B, Sreenivasa G, Rau B, Gellermann J, Riess H, et al. Hyperthermia in combined treatment of cancer. Lancet Oncol 2002;3:487–97.
[2] van der Zee J. Heating the patient: a promising approach. Ann Oncol 2002;13:1173–84.
[3] Kennedy LC, Bickford LR, Lewinski NA, Coughlin AJ, Hu Y, Day ES, et al. A new era for cancer treatment: gold-nanoparticle-mediated thermal therapies. Small 2011;7:169–83.
[4] Chen CC, Lin YP, Wang CW, Tzeng HC, Wu CH, Chen YC, et al. DNA-gold nanorod conjugates for remote control of localized gene expression by near infrared irradiation. J Am Chem Soc 2006;128:3709–15.
[5] Kuo TR, Hovhannisyan VA, Chao YC, Chao SL, Chiang SJ, Lin SJ, et al. Multiple release kinetics of targeted drug from gold nanorod embedded polyelectrolyte conjugates induced by near-infrared laser irradiation. J Am Chem Soc 2010;132:14163–71.
[6] Kam NWS, O'Connell M, Wisdom JA, Dai HJ. Carbon nanotubes as multifunctional biological transporters and near-infrared agents for selective cancer cell destruction. Proc Natl Acad Sci U S A 2005;102:11600–5.
[7] Yang K, Zhang SA, Zhang GX, Sun XM, Lee ST, Liu ZA. Graphene in mice: ultrahigh in vivo tumor uptake and efficient photothermal therapy. Nano Lett 2010;10:3318–23.
[8] Robinson JT, Tabakman SM, Liang YY, Wang HL, Casalongue HS, Vinh D, et al. Ultrasmall reduced graphene oxide with high near-infrared absorbance for photothermal therapy. J Am Chem Soc 2011;133:6825–31.
[9] Chou SW, Shau YH, Wu PC, Yang YS, Shieh DB, Chen CC. In vitro and in vivo studies of FePt nanoparticles for dual modal CT/MRI molecular imaging. J Am Chem Soc 2010;132:13270–8.
[10] Latham AH, Williams ME. Controlling transport and chemical functionality of magnetic nanoparticles. Acc Chem Res 2008;41:411–20.
[11] Seehra MS, Singh V, Dutta P, Neeleshwar S, Chen YY, Chen CL, et al. Size-dependent magnetic parameters of fcc FePt nanoparticles: applications to magnetic hyperthermia. J Phys D Appl Phys 2010;43:145002–8.
[12] Chou SW, Zhu CL, Neeleshwar S, Chen CL, Chen YY, Chen CC. Controlled growth and magnetic property of FePt nanostructure: cuboctahedron, octapod, truncated cube, and cube. Chem Mater 2009;21:4955–61.
[13] Tong L, Zhao Y, Huff TB, Hansen MN, Wei A, Cheng JX. Gold nanorods mediate tumor cell death by compromising membrane integrity. Adv Mater 2007;19:3136–41.
[14] Bagaria HG, Ada ET, Shamsuzzoha M, Nikles DE, Johnson DT. Understanding mercapto ligand exchange on the surface of FePt nanoparticles. Langmuir 2006;22:7732–7.
[15] Lu YJ, Low PS. Folate-mediated delivery of macromolecular anticancer therapeutic agents. Adv Drug Deliv Rev 2002;54:675–93.
[16] Kotaidis V, Plech A. Cavitation dynamics on the nanoscale. Appl Phys Lett 2005;87:213102–4.
[17] Lin CP, Kelly MW. Cavitation and acoustic emission around laser-heated microparticles. Appl Phys Lett 1998;72:2800–2.
[18] Chen CL, Kuo LR, Chang CL, Hwu YK, Huang CK, Lee SY, et al. In situ real-time investigation of cancer cell photothermolysis mediated by excited gold nanorod surface plasmons. Biomaterials 2010;31:4104–12.
[19] Richardson HH, Carlson MT, Tandler PJ, Hernandez P, Govorov AO. Experimental and theoretical studies of light-to-heat conversion and collective heating effects in metal nanoparticle solutions. Nano Lett 2009;9:1139–46.
[20] Zharov VP, Galitovskaya EN, Johnson C, Kelly T. Synergistic enhancement of selective nanophotothermolysis with gold nanoclusters: potential for cancer therapy. Lasers Surg Med 2005;37:219–26.
[21] American national standard for safe use of lasers ANSI Z136.1. Orlando, Florida: American Laser Institute; 2000.
[22] Fischer M, Georges J. Prediction of the calibration curves for the analysis of high absorbances using mode-mismatched dual-beam thermal lens spectrometry with chopped continuous wave laser excitation. Anal Chim Acta 1996;322:117–30.
[23] Shen J, Lowe RD, Snook RD. A model for cw laser induced mode-mismatched dual-beam thermal lens spectrometry. Chem Phys 1992;165:385–96.
[24] Hessel CM, Pattani VP, Rasch M, Panthani MG, Koo B, Tunnell JW, et al. Copper selenide nanocrystals for photothermal therapy. Nano Lett 2011;11:2560–6.
[25] Ekici O, Harrison RK, Durr NJ, Eversole DS, Lee M, Ben-Yakar A. Thermal analysis of gold nanorods heated with femtosecond laser pulses. J Phys D Appl Phys 2008;41:185501–11.
[26] Rudnitzki F, Bever M, Rahmanzadeh R, Brieger K, Endl E, Groll J, et al. Bleaching of plasmon-resonance absorption of gold nanorods decreases efficiency of cell destruction. J Biomed Opt 2012;17:058003–16.